Characterization of the Solution Conformations of Unbound and Tat Peptide-Bound Forms of HIV-1 TAR RNA†

Katherine S. Long and Donald M. Crothers*

Department of Chemistry, Yale University, New Haven, Connecticut 06520-8107

Received March 15, 1999; Revised Manuscript Received May 24, 1999

ABSTRACT: Basic peptides from the carboxy terminus of the HIV-1 Tat protein bind to the apical stem−loop region of TAR RNA with high affinity and moderate specificity. The conformations of the unbound and 24 residue Tat peptide (Tfr24)-bound forms of TAR RNA have been characterized by NMR spectroscopy. The unbound form of TAR exists in major and minor forms having different trinucleotide bulge conformations. A specific TAR RNA conformational change is observed upon complex formation with Tfr24, consisting of coaxial stacking of helical stems and base triple formation. A U23-A27-U38 base triple is proposed based on exchangeable proton NMR data, where U23 forms a base pair with A27 in the major groove. No evidence for base triple formation was found for Tat peptides in which lysine residues are extensively substituted for arginine.

The Tat protein from human immunodeficiency virus type 1 (HIV-1) is a potent transactivator (*1*) and is essential for viral replication (*2*). Tat activates transcription during the early phase of viral gene expression, where the doubly spliced pre-messenger RNAs encoding the regulatory proteins Tat, Rev, and Nef are expressed (*3*, *4*). Tat stimulates transcription after binding the transactivation response element or TAR RNA, found at the 5′ end of all pre-messenger RNA transcripts (*5*). The functional importance of the Tat−TAR interaction to the viral life cycle makes it an attractive target for intervention with antiviral agents. Thus, elucidation of the three-dimensional solution structure of the complex will aid in the rational design of therapeutic drugs.

Carboxy-terminal fragments of Tat, including an arginine-rich region, bind to a shortened form of TAR (ΔTAR) spanning a trinucleotide bulge with subnanomolar affinity (*6*). Modification interference experiments have mapped the TAR RNA contact site to the trinucleotide bulge region and adjacent base pairs (*6*). For sequence-specific interaction, the two base pairs above the bulge (G26-C39 and A27-U38) as well as a bulge of at least two nucleotides with a uridine residue at the base of the bulge are required (*7*, *8*). Several phosphate groups adjacent to the bulge, including P21 (between G21 and A22), P22, and P40, are essential for RNA recognition by Tat as indicated by interference experiments (*9*, *7*) and methylphosphonate substitutions (*10*).

A series of experiments by Frankel and co-workers have demonstrated that TAR RNA contains a specific arginine binding pocket (*11*). Short arginine homopolymers bound TAR specifically when compared with lysine analogues (*12*). Additionally, mutants of the Tat protein containing a basic region composed entirely of arginine or a single central arginine elicited wild-type transactivation levels (*9*). L-Arginine was able to compete with a Tat-derived peptide for TAR binding (*13*), and a similar CD signal change was observed upon addition of arginine or Tat peptide to TAR RNA (*14*). NMR studies of a HIV-1 TAR−argininamide complex showed that TAR undergoes a conformational change upon argininamide binding and identified a specific arginine binding site in the major groove near G26 (*15*). The proposed model included base triple formation of U23 with the A27-U38 base pair above the bulge in the bound form of TAR (*15*). Compelling evidence for the base triple model was obtained through a series of mutants which were either incapable or capable of base triple formation, including an isomorphous base triple mutant ($C23^+$-G27-C38) (*16*). Additional evidence from exchangeable protons was obtained in subsequent investigations of HIV-2 TAR−argininamide complexes (*17*, *18*).

The NMR investigations of another research group have focused on the conformations of TAR RNA in the unbound state, bound to argininamide, and bound to several peptides (*19*, *20*). One of the peptides used is largely analogous to Tfr24 described in this work, while the other includes additional residues from the core domain (*19*). A TAR RNA conformational change involving stacking between A22 and G26 was reported in the presence of both argininamide and peptides. These studies position U23 in the major groove near G26 and A27; however, no evidence of base triple formation was observed.

First observed in crystal structures of tRNA, base triples are an important structural element in that they impose strong constraints on the three-dimensional fold of RNA molecules (*21*). Base triples have appeared in several related RNA structures including the HIV-1 Rev peptide−RNA aptamer complex, where a U23-A26-U9 base triple is observed with the Hoogsteen base-paired U23 sandwiched between two arginine side chains (*22*). In this case, an NOE between the imino proton of U23 and the A26 H8 and resolved A26 amino protons was observed. Of two NMR investigations of the BIV Tat−TAR complex (*23*, *24*), one only detects evidence for a U-A-U base triple under conditions of lowered

† Supported in part by NIH Grant GM21966.

10.1021/bi990590h CCC: $18.00
Published on Web 07/10/1999

(a)

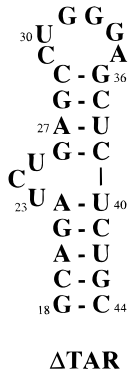

ΔTAR

(b)

Tfr24	RKKRRQRRRPPQGSQTHQVSLSKQ
R52	RKKRKQKKKPPQGSQTHQVSLSKQ
R52R53K54	RKKRRKKKKPPQGSQTHQVSLSKQ

FIGURE 1: HIV-1 ΔTAR RNA and Tat-derived peptide sequences used in NMR structural studies. (a) The secondary structure of ΔTAR RNA is depicted with positions numbered (5′ to 3′) from G18 to C44, with position +1 denoting the transcription start site. (b) Twenty-four amino acid peptides include Tfr24 (*6*), which has the wild-type Tat sequence, and the Tfr24-derived peptides R52 and R52R53K54 (*31*).

pH and temperature (*24*). A category of base triples, including those in bound HIV-1 and BIV TAR RNAs, are more susceptible to exchange with solvent and, like terminal base pairs, are observable only under lowered temperature and pH conditions.

In the present work, the solution conformations of the unbound and 24 residue Tat peptide-bound forms of TAR are examined. In the unbound state, major and minor conformers of TAR are observed with different stacking arrangements at the trinucleotide bulge. Identification of the minor form provides an explanation for the moderate specificity of Tat peptides for TAR, especially at higher concentrations, wherein a particular bulge conformation is recognized in specific complex formation. In the bound form of TAR, exchangeable proton NMR evidence for base pairing of U23 with A27-U38 is presented. Additional data are provided by (*25*). The model for base triple formation supported by our data, through Hoogsteen base pairing of U23 with A27 in the major groove, provides a rationale for the essential role of U23 in both specific complex formation with Tat and, thereby, transactivation of viral gene expression.

MATERIALS AND METHODS

NMR Sample Preparation. The 27 nucleotide HIV-1 ΔTAR RNA sequence (Figure 1a) of the HIV-1_{HXB2R} isolate (*26*) was used in all NMR samples, except that the terminal base pair was changed from C-G to G-C to increase transcription yields. Samples of ΔTAR RNA were prepared through in vitro transcription reactions using T7 RNA polymerase (*27*, *28*). Uniformly labeled NMR samples of ΔTAR were enzymatically synthesized from ^{15}N- or ^{13}C,^{15}N-enriched ribonucleotide triphosphates prepared from RNA isolated from *Escherichia coli* grown on media with [^{15}N]-ammonium chloride and [^{13}C]glucose as the sole nitrogen and carbon sources, respectively. The exact protocol used was derived from those described by Pardi (*29*), Williamson (*30*), and their co-workers.

Purified RNA samples were dialyzed extensively against 10× and then against 1× NMR buffer (15 mM sodium cacodylate, pH 6.2, 0.15 mM EDTA). Samples were annealed by heating to 50 °C and then cooling on ice. Final sample concentrations ranged between 1.0 and 1.5 mM. Samples were examined in either standard (Wilmad) or Shigemi NMR tubes (Shigemi) and were resuspended either 90% water/10% deuterium oxide (Cambridge Isotope Laboratories) or 99.996% deuterium oxide (Isotec).

The Tfr24 peptide has the Tat protein sequence of the HIV-1_{BRU} isolate (*31*). The R52 and R52R53K54 peptides were designed from the context of the wild-type Tfr24 sequence (*32*). Peptides were chemically synthesized on an Applied Biosystems Model 430A peptide synthesizer using standard procedures. Peptides were purified by reverse-phase HPLC, characterized by mass spectrometry, and dialyzed as described for the RNA samples. The concentration of peptide stock solutions was determined through amino acid analysis. The NMR samples used in these studies included: (1) unlabeled ΔTAR RNA, (2) ^{15}N-ΔTAR, (3) ^{13}C,^{15}N-ΔTAR, (4) unlabeled Tfr24−ΔTAR, (5) Tfr24−^{15}N-ΔTAR, (6) Tfr24−^{13}C,^{15}N-ΔTAR, (7) R52−^{15}N-ΔTAR, and (8) R52R53K54−^{15}N-ΔTAR.

NMR Spectroscopy. NMR experiments were collected on Bruker AM 500 MHz, General Electric Omega 500 MHz, and Varian Unity Plus 600 MHz spectrometers. Data were transferred to Silicon Graphics workstations and processed using the FELIX 95 software package (Biosym Technologies, Inc., San Diego). Proton chemical shifts were referenced to water at 4.8 and 4.68 ppm relative to tetramethylsilane at 15 and 25 °C, respectively. Nitrogen and carbon chemical shifts were referenced internally by setting the heteronuclear carrier frequency to an appropriate value in the center of the spectrum.

Standard NOESY *(33)* and DQF-COSY (*34*) experiments were performed on unlabeled samples of ΔTAR RNA and the Tfr24−ΔTAR complex. In NOESY experiments, presaturation was used to suppress the residual water peak. Datasets were collected with mixing periods of 50, 100, 200, and 300 ms. Two-dimensional NOESY experiments in water were collected with jump−return spin−echo water suppression (*35*) and mixing times of 200−400 ms. Two-dimensional ^{15}N−^{1}H HMQC experiments (*36*, *37*) were collected on samples containing uniformly ^{15}N-enriched ΔTAR. These included one-bond nitrogen correlation experiments for imino and amino protons, and a two-bond ^{15}N−^{1}H HMBC experiment. ^{13}C−^{1}H HSQC experiments were collected at 15 and 25 °C for ^{13}C,^{15}N-ΔTAR and at 15 °C for the Tfr24−^{13}C,^{15}N-ΔTAR complex. The ^{13}C−^{1}H HSQC experiments on the Tfr24−ΔTAR complex were collected in water, using a watergate − water flip-back water suppression scheme (*38*−*40*). In all heteronuclear experiments, GARP was used to decouple heteronuclei during acquisition (*41*).

Constraints for Structure Determination. Where all available evidence suggested a canonical A-form helical structure, model A-form distances were used to increase the number of generated structures that satisfied all of the experimental constraints. The appropriate helical stem of ΔTAR was built using the biopolymer module of the Insight II 95.0 software package (Biosym/MSI, San Diego, CA). A file of distances was generated from the Insight model and converted into a format suitable for input into the structure calculation.

Experimental NMR distance and torsion angle constraints for the unbound and bound forms of ΔTAR RNA were obtained from NOESY and COSY spectra using standard methods. NOE cross-peaks of medium to strong intensity in experiments with 50, 100, and 200 ms NOESY mixing times were put into 2.3 ± 0.7 (short), 2.8 ± 1.2 (medium), and 3.8 ± 2.2 Å (long) distance categories, respectively. Cross-peaks involving exchangeable protons were usually assigned to the long distance category to reduce possible bias due to differential exchange rates with solvent or nonuniform excitation profiles (*42*). The glycosidic torsion angle was usually constrained to the anti range and only constrained to the syn range in cases where a very strong intranucleotide aromatic H6/H8 to anomeric H1′ proton NOE was observed. The angle was left unconstrained in a few cases made ambiguous due to spectral overlap. The torsion angles in the ribose ring were constrained according to qualitative determinations of sugar pucker from DQF-COSY spectra. If no H1′−H2′ cross-peak was present in the DQF-COSY spectrum, the ribose torsion angles were constrained to have C3′-endo sugar pucker values. Since explicit *J*-coupling values were not measured, a nucleotide with a visible H1′−H2′ cross-peak was interpreted as one which sampled the C2′-endo conformation a certain percentage of the time. The sugar torsion angles of such nucleotides were left unconstrained. The backbone torsion angles were constrained to their standard A-form values in canonical helical stem regions. In the bulge and loop regions of ΔTAR RNA, these torsion angles were left unconstrained. In addition, the torsion angle flexibility was increased in noncanonical regions and in the two adjacent base pairs on either side of the ΔTAR trinucleotide bulge. The sugar and backbone torsion angle ranges of nucleotides in these regions were increased from 10° to 30° and from 20° to 45°, respectively.

Hydrogen bonding constraints were used in cases where both a stable imino proton and an NOE cross-peak from an imino to aromatic or amino proton between base-paired nucleotides were observed. One exception to the above conditions was the terminal G-C base pair of ΔTAR. Another exception was the A22-U40 base pair in the unbound form of ΔTAR, for which no imino proton is observed. The U40 imino proton exists in an environment where it is exposed to rapid solvent exchange, although several pieces of evidence from nonexchangeable spectra suggest that this base pair is formed.

Standard interatomic distances for Watson−Crick base pairs were obtained from those observed in crystal structures of GpC and ApU (*43*). The Hoogsteen base pair between U23 and A27 in the U23-A27-U38 base triple in the bound form of ΔTAR was modeled using distances observed in a crystal structure of 9-ethyladenine-1-methyl-5-iodoracil (*44*).

Planarity restraints were imposed on base-paired nucleotides to minimize propeller twisting between bases. A force constant of 50 kcal·mol^{-1}·Å^{-2} was used to impose planarity between the two base planes, defined by the N1, N3, and C5 atoms on both nucleotides. For the initial set of calculations, a planarity restraint was not imposed on the third nucleotide of the base triple, U23, in the bound form of ΔTAR. This was done to observe the range of structures generated from the experimental restraints. The planarity constraint on U23 was imposed, however, in model calculations to generate a more ideal base triple. The planarity restraint for the A22-U40 base pair in the bound form of ΔTAR was reduced to 5 kcal·mol^{-1}·Å^{-2} or removed to extract a longer A22 H2 to G26 H1′ same-strand distance compared to the cross strand A22 H2 to C41 H1′ distance, that is apparent from the experimental NMR data.

Calculation of Model Structures. Structure calculations were carried out using the XPLOR version 3.1 software package (*45*). The nucleic acid parameter and topology files of XPLOR (*46*) and the primary structure of ΔTAR were used to generate energy-minimized starting templates. A distance geometry routine was used to produce a three-dimensional model with an overall fold consistent with the information contained in the NOE, torsion angle, hydrogen bonding, and planarity constraint files.

Several rounds of a simulated annealing protocol were used to refine the structures afforded from distance geometry. The protocol included 200 rounds of initial energy minimization, followed by 3 ps of restrained molecular dynamics at 3000 K. Another set of restrained molecular dynamics was carried out as the system was cooled to 100 K in 3 ps. The system was cooled in 58 cooling cycles with a temperature increment of 50 K. Attractive electrostatic or van der Waals energy terms were not included in the calculations. The protocol concluded with 800 rounds of final energy minimization. Where included, the force constants used for the NOE and dihedral angle constraint terms were 100 kcal·mol^{-1}·Å^{-2} and 200 kcal·mol^{-1}·rad^{-2}, respectively. The threshold values for NOE and torsion angle violations were 0.5 Å and 5°, respectively.

Each final structure was generated from a different round of distance geometry with one to three subsequent rounds of simulated annealing. The structures selected for analysis were only those which had no distance or torsion angle violations. Structures which satisfied the experimental constraints were examined in terms of their energies and stereochemistry. Insight II 95.0 was used to analyze individual structures and superimpose families of structures to obtain RMSD values.

RESULTS

Major and Minor ΔTAR RNA Conformers Exist in the Unbound State. Standard methods were used to trace base pairing and base stacking patterns in unbound ΔTAR RNA [Figure 1(a)]. Sequential connectivities between H6/H8 and H1′ protons were observed from G18 to C24. The sequential walk was interrupted at U25, and then continued from G26 to C29. The degree of stacking between nucleotides in the trinucleotide bulge, evidenced by the number of sequential NOE cross-peaks, progressively decreased from 5′ to 3′. The relatively few interresidue NOE cross-peaks that are observed in the loop indicate that these nucleotides are largely unstacked. On the 3′ side of the hexanucleotide loop, uninterrupted sequential connectivities were observed between G36 and C44.

The positions of the four adenine H2 protons in ΔTAR were verified using ^{13}C−^{1}H HSQC and ^{15}N−^{1}H HMBC experiments [Figure 2d(a)]. In addition to four major sets of H2 correlations observed in the ^{15}N−^{1}H HMBC experiment, a minor set was observed at 7.64 ppm [Figure 2(a)]. An alternate conformer was discovered upon reconciliation of

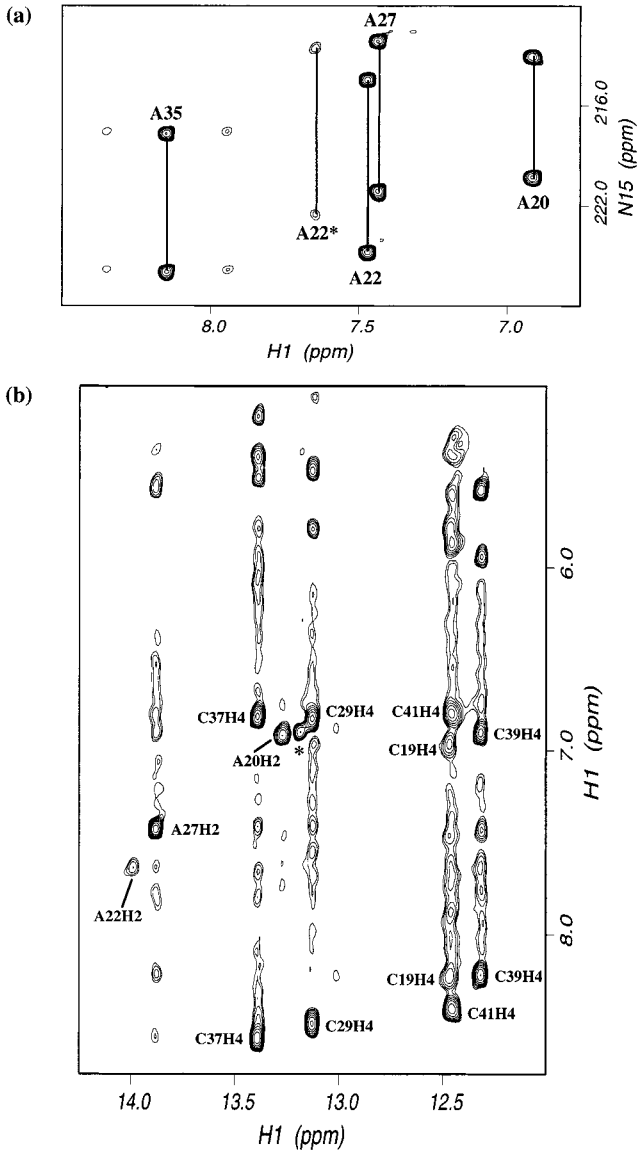

FIGURE 2: NMR spectra of unbound ΔTAR RNA. (a) Positions of adenine H2 resonances in ΔTAR RNA in an HMBC experiment at 25 °C. The A22 correlation denoted with an asterisk is a minor, Watson−Crick base-paired form of A22. (b) Imino−amino, aromatic proton region of a NOESY experiment in water at 15 °C. The asterisk denotes an NOE to A20 H2 from a minor form of U42 H3.

exchangeable and nonexchangeable spectral data. Sequential imino−imino proton cross-peaks were observed in the upper stem of ΔTAR, but ceased at the junction between upper and lower helical stems (data not shown). The only candidate for the U40 imino proton was the resonance at 14.04 ppm, which had a NOE to an A H2 proton at 7.64 ppm [Figure 2(b)]. However, the A22 H2 proton was assigned at 7.45 ppm from nonexchangeable spectra [Figure 2(a)]. Hence, the major form of the A22-U40 base pair does not have an observable U40 imino proton. However, the A22-U40 base pair is, nevertheless, in a Watson−Crick base pairing arrangement. Both A22 and U40 nucleotides can be traced in standard aromatic−anomeric sequential walks. In addition, same- and cross-strand NOEs are observed from A22 H2 to U23 and C41 H1′ protons, respectively.

The data suggest that the major form of unbound ΔTAR exists in an open conformation in the trinucleotide bulge region, whereby the U40 imino proton is susceptible to rapid exchange with solvent. The resonance at 14.04 ppm is assigned to a minor conformer of ΔTAR, where the U40 imino proton is stable to exchange with solvent (Figure 2). The resonances corresponding to the minor form of the A22-U40 base pair are of weak intensity relative to the two other A-U base pairs in the NOESY spectrum [Figures 2(b)]. This is consistent with the small percentage of RNA adopting this conformation, as evidenced by the relative intensity of correlations observed in the $^{15}N-^{1}H$ HMBC experiment [Figure 2(a)].

Additional non-hydrogen-bonded imino protons corresponding to G and U nucleotides in the loop and bulge are observed in $^{15}N-^{1}H$ HMQC experiments (data not shown). Three resonances corresponding to the loop G imino protons are observed between 10.5 and 11.6 ppm. Although only three U imino resonances are expected from the sequence, five peaks are observed. This indicates that there are multiple conformations of the trinucleotide bulge that are in slow exchange on the NMR time scale. These conformations are likely ones in which different nucleotides are stacked between the two helices. At lower temperatures, two resonances become much more intense, suggesting that at least one conformation becomes protected from solvent exchange, possibly one in which U23 is stacked between the two helices.

Formation of the Tfr24−ΔTAR Complex. Peptide−ΔTAR RNA complexes were prepared by stepwise titration of an equimolar amount of peptide [Figure 1(b)] to ΔTAR RNA. Complex formation with unlabeled and labeled ΔTAR RNA was followed by monitoring the imino proton region with either 1D proton spectra or 2D $^{15}N-^{1}H$ HMQC experiments, respectively, at 15 °C. The principal marker for Tfr24−ΔTAR complex formation was the appearance of a well-separated, downfield resonance at 14.28 ppm [Figure 3(c)]. Another marker was the appearance of an additional hydrogen-bonded U imino proton at 13.67 ppm. Two out of three base-paired U's displayed downfield proton chemical shift changes upon complex formation [Figure 3(a),(c)]. In addition, modest upfield shifts of several G imino nitrogens were observed [Figure 3(b),(d)].

An important issue to be addressed with regard to complex formation is the specificity of the interaction between Tfr24 and ΔTAR. Titration experiments were originally designed so that the final concentration of complex would be approximately 1 mM. At the point in the titration where the molar ratio of peptide to RNA was approximately 1:1, the spectrum appeared more like a titration step at 3:4 peptide to RNA (data not shown). At the titration step where the calculated molar ratio of peptide to RNA was 1:1, residual peaks present in the RNA spectrum alone remained, and the additional U imino proton and other markers for specific complex formation were not full resonances. If additional peptide was added in small titration steps, the markers of specific complex formation disappeared, indicating that the RNA sample had been overtitrated with peptide (data not shown).

An equimolar peptide−RNA complex can be formed at nanomolar concentrations in electrophoretic mobility shift assays. However, the partition coefficients which describe the behavior of this system are apparently concentration dependent. If titrations were carried out so that the final

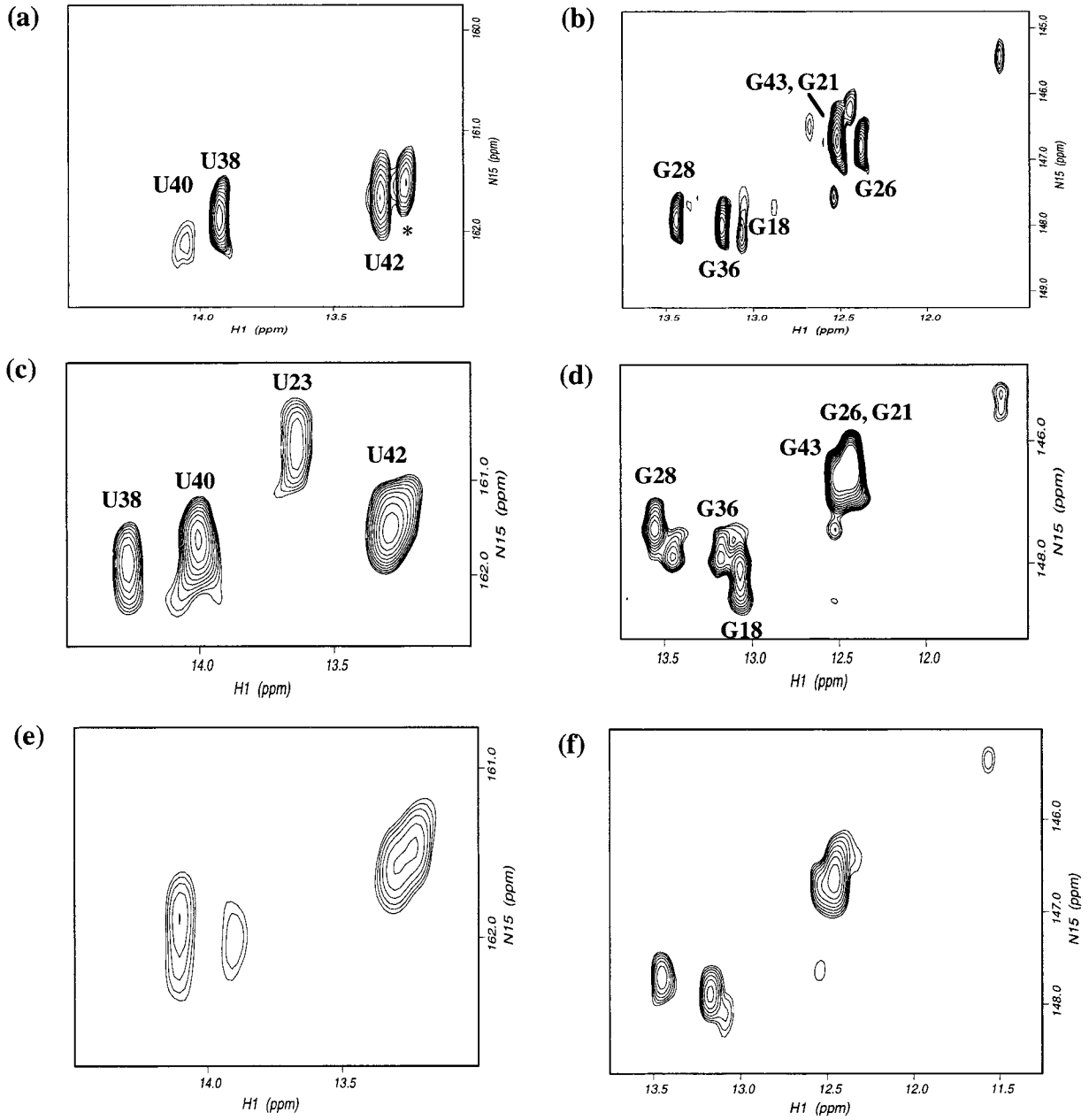

FIGURE 3: Sections from two-dimensional $^{15}N-^{1}H$ HMQC spectra of titration experiments to form the Tfr24−ΔTAR complex at 15 °C. Panels (a)−(b), (c)−(d), and (e)−(f) are of ΔTAR, the Tfr24−ΔTAR complex, and the R52−ΔTAR complex, respectively. Panels (a), (c), and (e) are U and (b), (d), and (f) are G imino proton−nitrogen regions. The ΔTAR samples are $^{13}C,^{15}N$-labeled in (a)−(b) and ^{15}N-labeled in (c)−(f). The peak denoted with an asterisk is a contaminating form of U42 from the in vitro transcription reaction.

concentration of complex was about 0.6 mM, a specific 1:1 complex could be formed [Figure 3(c),(d)]. At higher concentrations, a detectable population of peptide is bound nonspecifically to ΔTAR, possibly by binding RNA with an alternative bulge conformation. The concentration dependence of the phenomenon implies a role for aggregation effects. Thus, there appears to be a concentration "ceiling" of approximately 0.6 mM for specific complex formation.

The peptide−ΔTAR RNA complexes R52R53K54−ΔTAR and R52−ΔTAR were found to have intermediate and low kinetic stabilities relative to the wild-type complex, respectively (*32*). To put the kinetic behavior of these systems into a structural context, the base pairing interactions in these complexes were probed and compared to those observed in ΔTAR RNA and the Tfr24−ΔTAR complex. Complexes were formed in a fashion similar to the wild-type complex, via titration of R52R53K54 and R52 peptides [Figure 1(b)] to ^{15}N-ΔTAR to form an equimolar complex. Portions of the 2D $^{15}N-^{1}H$ HMQC spectra at 1:1 R52 peptide:ΔTAR RNA are shown in Figure 3(e),(f). For both complexes, the markers observed for specific complex formation in the wild-type complex are absent [Figure 3(e),(f); and data not shown].

NMR Assignment of the Bound Form of ΔTAR in the Tfr24−ΔTAR Complex. The sequential aromatic−anomeric walk in the bound form of ΔTAR was traced from G18 through A22, and from G26 through C29 (Figure 4). U23 is not stacked on A22 in the bound form of ΔTAR, as evidenced by nonsequential A-form stacking between A22 and G26 (Figure 4). The connectivities are interrupted at the hexanucleotide loop and then resume at G36, continuing through C44 at the 3′ end. Similar connectivity pathways can be traced at both 15 and 25 °C (data not shown). Standard

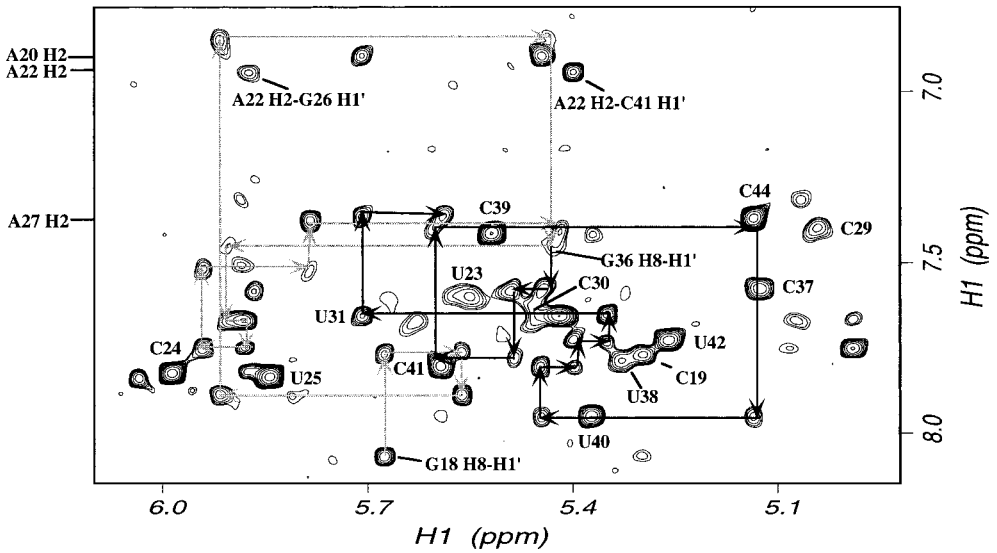

FIGURE 4: NOESY NMR spectra of ΔTAR bound in the Tfr24−ΔTAR complex at 15 °C. The aromatic−anomeric sequential walk between H6/H8 and H1′ protons is traced for both 5′ purine-rich (gray) and 3′ pyrimidine-rich (black) portions of ΔTAR. Tracings for both strands are in the 5′ to 3′ direction. Continuous sequential connectivities are observed from G18 to A22, from A22 to G26, and from G26 to C29 in the purine-rich strand and from G36 to C44 in the pyrimidine-rich strand. Pyrimidine H5−H6 cross-peaks and the starting points for both strand tracings are labeled.

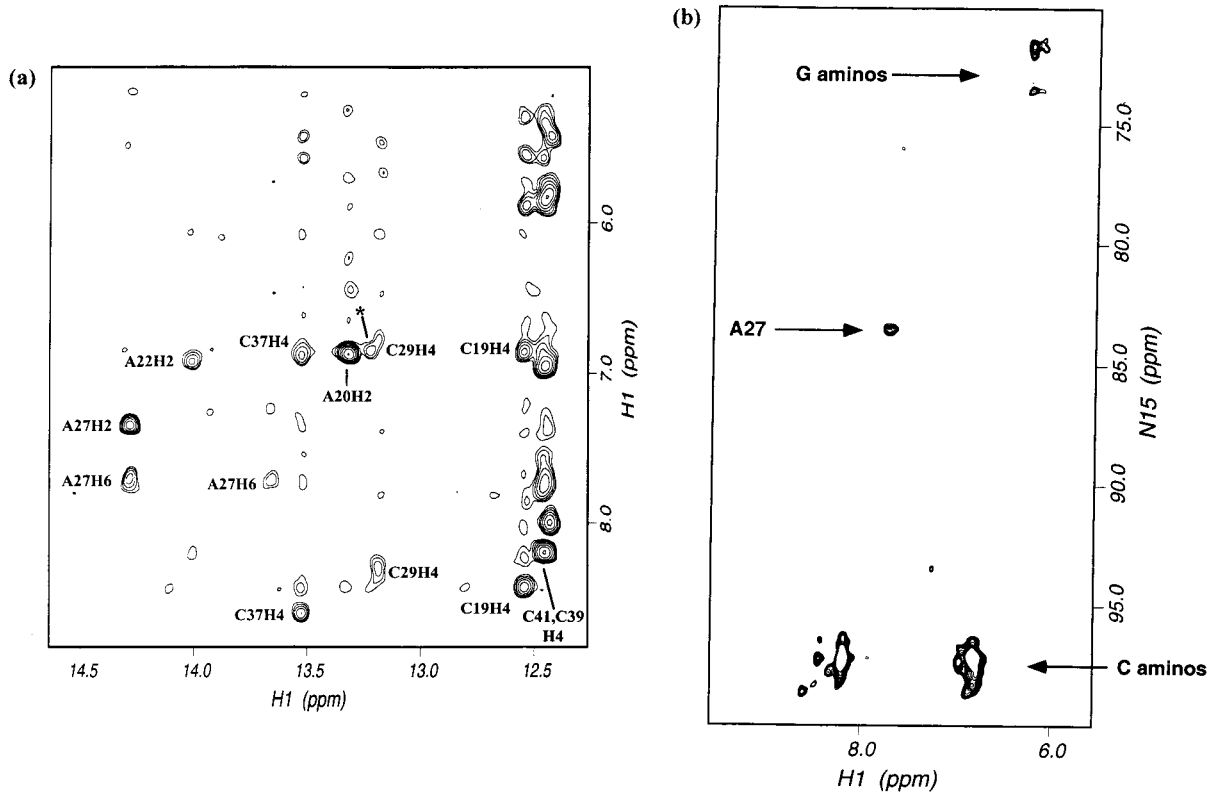

FIGURE 5: Exchangeable proton NMR spectra of ΔTAR bound in the Tfr24−ΔTAR complex at 15 °C. (a) Imino−amino, aromatic proton regions of a NOESY experiment. The asterisk in (a) denotes a minor population of the A20-U42 base pair. (b) Amino proton−nitrogen region of an $^{15}N-^{1}H$ HMQC experiment.

NOEs for A-form RNA are observed from A20 and A27 H2 protons to the respective H1′ protons on the same- and cross-strand 3′ nucleotides. In canonical A-form geometry, the distances from A H2 to 3′ nucleotide H1′ protons on the same- and cross-strands are both about 4 Å (*47*). In the case of the A22 H2 proton, the same-strand NOE to the G26 H1′ proton is significantly weaker than the NOE to the cross-strand C41 H1′ proton (Figure 4). This deviation from normal relative H2 to H1′ cross-peak intensities indicates that there is a distortion in the local geometry of the A22-U40 base pair at the site of coaxial stacking.

Upon addition of the wild-type peptide to ΔTAR RNA, an extra U imino proton appears in the spectrum of the complex. The proton chemical shift (13.67 ppm) indicates that the imino proton is involved in a hydrogen bond [Figures 3(c) and 5(a) and data not shown]. The nitrogen chemical shift (160.7 ppm) is about 1 ppm upfield of other U nucleotides involved in Watson−Crick base-pairing

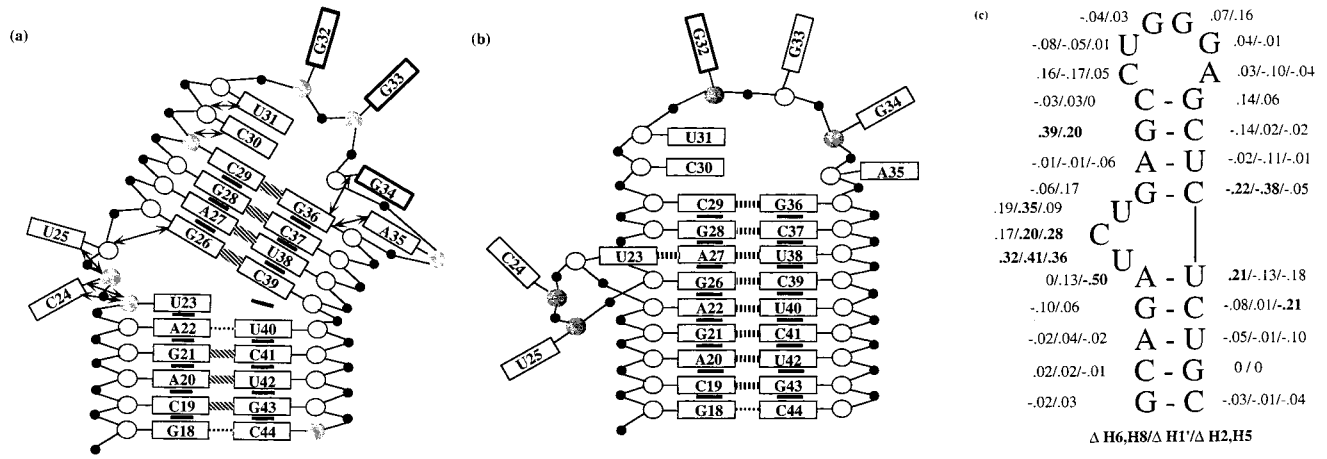

FIGURE 6: Summary of NMR data. Panels (a) and (b) are schematic diagrams of unbound and bound forms of ΔTAR RNA, respectively. Nucleotide bases, ribose moieties, and phosphate groups are denoted by large rectangles, large circles, and small circles, respectively. A population of C2′-endo sugar conformation as indicated by observation of a H1′−H2′ cross-peak in the DQF-COSY spectrum is shown in shaded circles, whereas open circles denote a C3′-endo sugar conformation. Filled rectangles indicate base−base stacking. Canonical A-form helical stacking is observed between C39 and U40. The hatched lines indicate hydrogen bonding between bases. The dashed lines denote base pairs with imino protons that are weak or unobserved due to fast exchange rates with solvent. In (b), the ribose sugar of A27 and the phosphate group between G26 and A27 have been omitted for clarity. (c) Schematic diagram of ΔTAR RNA labeled with the H6, H8/H1′/H2, H5 proton chemical shift changes observed at each nucleotide upon complex formation. The chemical shift changes are reported as $\nu_{bound} - \nu_{unbound}$.

[Figure 3(c)]. This upfield shift is consistent with those observed for T imino nitrogens involved in Hoogsteen base pairing in T-A-T base triples in pyrimidine-purine-pyrimidine DNA triplexes (*48*).

The additional imino proton does not have NOEs to any other imino proton, but an NOE is observed to a proton at 7.71 ppm [Figure 5(a)]. There is also an NOE at the same chemical shift involving the U38 imino proton. An HMQC experiment positively identifies this proton as the A27 amino proton [Figure 5(b)]. The analogous HMQC experiment on ^{15}N−ΔTAR yielded no observable amino resonances from A nucleotides (data not shown). The A27 amino proton of Tfr24−ΔTAR is observed due to a decrease in the solvent exchange rate because of participation in a hydrogen bond with a uridine in addition to U38. The results show that two uridine imino protons are within NOE detection distance of the A27 amino proton. A model that is consistent with the NMR and biochemical data is that U23 forms a base triple through a hydrogen bond with the A27 amino proton. Models of bound ΔTAR RNA generated from experimental NMR data reveal that the distances from the U23 imino proton to the A27 amino and H8 protons are comparable. Since the chemical shifts of the A27 amino and H8 protons are similar and the cross-peak in question is broad, we cannot rule out that there is also an NOE between the U23 imino and the A27 H8 protons at this position.

The assignment of the ΔTAR RNA bulge resonances was aided by phylogenetic and biochemical data which point to an essential and unique role for U23. Two nucleotides in the bulge, identified as a C and a U, share similar dynamic properties and local environments. This is evidenced by two very strong H5−H6 correlations observed in NOESY and DQF-COSY experiments (Figure 4 and data not shown). The H5/H6 cross-peaks at 5.98/7.83 and 5.84/7.84 ppm are assigned to C24 and U25 nucleotides, respectively. The H5/H6 cross-peak at 5.55/7.61 ppm is assigned to U23. Upon reexamination of the NOESY spectrum collected in water, NOEs are observed from the A27 amino proton to both the U23 H5 and H1′ protons (data not shown).

Due to the presence of two uridine nucleotides in the bulge, unambiguous evidence from NMR was sought to identify the U23 imino proton as the participant in the base triple with A27-U38. All approaches were hampered by the low sample concentration required to form a specific complex and the increased susceptibility of the U23 imino proton to solvent exchange. Extensive efforts to implement the triple resonance HNCCCH experiment described by Mueller and colleagues (*49*) were unsuccessful. The HNCCCH pulse sequence, designed to correlate U H3 and H6 protons, is comprised of four INEPT-type transfer steps and an N−C TOCSY mixing period. It is likely that the lengthy HNCCCH pulse train occurs in a time comparable to the overall T_2 relaxation time for the Tfr24−ΔTAR complex. A second approach was to obtain through-bond correlations in the uracil base using HNC and HCC experiments (J. P. Marino and C. Griesinger, manuscript in preparation). Here, the HNC experiment correlates U imino protons with C4 carbons, and the HCC experiment correlates H5 protons with C4 carbons. This experiment did not produce unambiguous correlations due to the very narrow chemical shift range of C4 (data not shown). Other possible experiments including HSQC−NOESY and ^{15}N-selected, ^{14}N-edited NOESY experiments were attempted but did not yield useful data.

Changes in RNA proton chemical shifts upon peptide binding are observed throughout the entire ΔTAR molecule, with the exception of the two terminal base pairs (Figure 6). The majority of significant chemical shift changes ($|\Delta\nu| \geq 0.2$ ppm) can be rationalized in terms of alterations in base stacking. A clustering of chemical shift changes occurs in nucleotides within or immediately adjacent to the trinucleotide bulge (Figure 6). The downfield chemical shift changes observed for U23, C24, and U25 are consistent with the unstacking of these nucleotides upon complex formation. Conversely, the significant upfield changes for A22 and C39

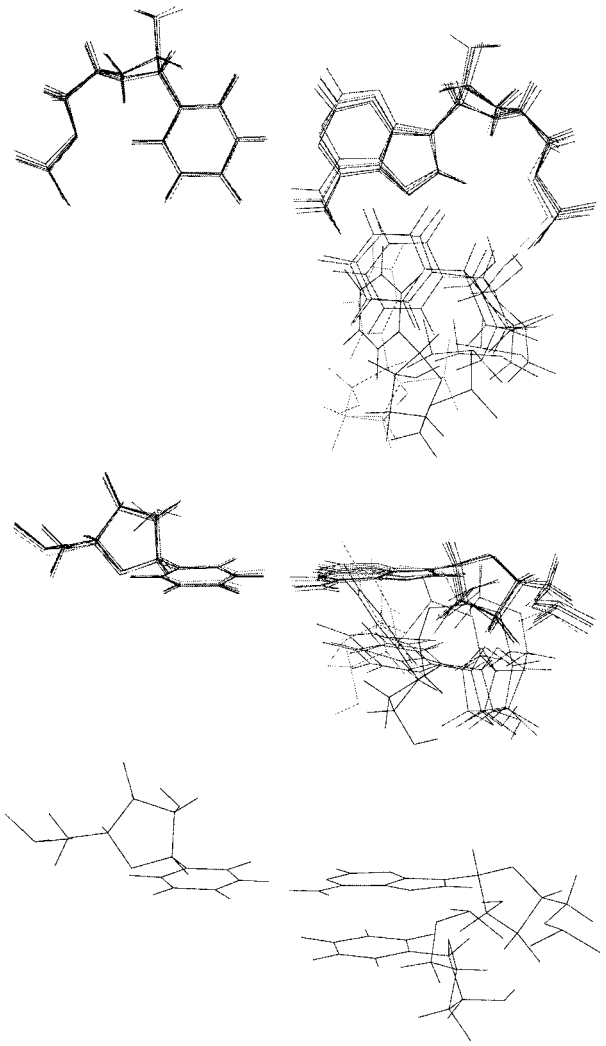

FIGURE 7: Views of the U23-A27-U38 base triple in calculated models of the bound form of ΔTAR RNA. Two views of the base triple for the five lowest energy structures superimposed on A27 and U38 are shown (top and middle). The base triple from the lowest energy structure from a model calculation with a planarity constraint imposed on U23 is shown for comparison (bottom).

are consistent with the stacking of base pairs involving these nucleotides upon Tat binding.

Modeling of the Base Triple. Models of the unbound and bound forms of ΔTAR were generated using experimental NMR data as described under Materials and Methods and are described in detail by (*25*). The present discussion will be limited to modeling of the base triple in the bound form of ΔTAR. Hydrogen bond constraints for Hoogsteen base pairing between U23 and A27 in a U23-A27-U38 base triple were included in the calculation of the bound structure. The criteria for inclusion of these constraints include the observation of a stable U23 imino proton, an NOE between the U23 imino and A27 imino protons, and an upfield-shifted U23 imino nitrogen resonance that is consistent with Hoogsteen base pairing.

The family of bound structures shows some variability in the exact position of the U23 base (Figure 7). Structures can be placed into two categories according to the relative placement of U23 with respect to A27 (Figure 7). One group consisted of the two lowest energy bound structures which had the plane of the U23 base at about a 60° angle relative to the plane of A27. In these two structures, the U23 H3 and O4 hydrogen bond donor and acceptor moieties were above and below the plane of the A27 base, respectively. In another group of structures, with an average total energy 17 kcal·mol^{-1} higher than the first group, the plane of the U23 ring was positioned slightly above that of A27.

To generate a U23-A27-U38 base triple with more ideal geometry, model calculations were performed on the bound form that included a planarity constraint between the U23 and A27 base planes (Figure 7). The convergence rate of the model calculations was comparable to those without the planarity constraint. The lowest energy structure from these calculations had a total energy between that of the two groups in the family of structures described above (Figure 7). The fact that structures of comparable energy can be generated with the inclusion of a U23 planarity restraint suggests that formation of an ideal base triple is possible. The experimental data collected in this investigation, however, are not sufficient to define an ideal base triple geometry for the bound form of ΔTAR.

Model Calculations. There are two U nucleotides in the wild-type HIV-1 TAR RNA trinucleotide bulge, U23 and U25. Despite phylogenetic and biochemical data that suggest an essential role for the 5′ bulge nucleotide, U23, it was not possible to obtain positive through-bond evidence from NMR that U23 is the participant in the base triple with A27-U38 in the bound form of ΔTAR. Consequently, model calculations were also performed with U25 as the nucleotide involved in the base triple. The model calculations were set up in an identical fashion as those for the bound form of ΔTAR, except that the identities of U23 and U25 were switched.

Out of a large number of initial structures generated from distance geometry, only 3% produced structures with no violations of the experimental constraints. The group of structures that satisfied the input constraints could be further subdivided into three groups based on energy. The high-energy group of structures had total energies that were approximately 3 times that of converged structures obtained in other calculations. These structures had a sharp bend between the two helical stems and a collapsed loop that interacted to different extents with the lower stem. A single structure of intermediate energy (468 kcal·mol^{-1}) had multiple base pairs with significant propeller twist. The two structures in the low-energy group suggest that it is possible to generate structures with U25 as the third nucleotide of the base triple. The energies of the U25 structures are somewhat higher than all of the converged structures obtained with U23 in the base triple and about 30 kcal·mol^{-1} higher in total energy. The convergence rate to acceptable structures for the U25 calculations was about 0.7%. The two sets of calculations where U25 or U23 were modeled as the third nucleotide in the base triple had the same number of experimental constraints; however, the convergence rate for the U25 calculations was much lower than those with U23. Although the results of these modeling calculations are not entirely conclusive, they support other data that suggest it is unlikely that U25 is the participant in the U-A27-U38 base triple.

DISCUSSION

The unbound ΔTAR RNA exists in two forms with different trinucleotide bulge conformations. In the major form, the 5′ bulge nucleotide, U23 is stacked upon the lower stem, whereas C24 and U25 adopt flexible conformations that are not well-defined by the NMR data. These data are in accord with work published by other laboratories on similar model ΔTAR RNAs (*20*, *15*), although an increased degree of stacking between C24 and U23 has been reported in an investigation conducted at higher salt concentration (*20*). The stacking patterns are consistent with ^{13}C relaxation measurements where calculated internal correlation times of aromatic bases of ΔTAR show an increase in relative mobility from 5′ to 3′ across the bulge nucleotides (*50*). They are also in agreement with a stronger ribonuclease A cleavage 3′ of C24 versus U23 (*51*).

In the major unbound form of ΔTAR, a stable imino proton is not observed for the A22-U40 base pair at the junction of the two helical stems. Chemical modification experiments with diethyl pyrocarbonate (DEPC) have shown that the purines in base pairs adjacent to the trinucleotide bulge in ΔTAR were accessible to DEPC, whereas the analogous residues in mutant ΔTAR sequences with one or no bulge nucleotides were not *(8)*. Bulges are known to introduce pronounced kinks into DNA, RNA, and hybrid DNA−RNA duplexes according to their number and relative position (*52*). Electrophoretic methods have shown that the asymmetric distribution of purines on one strand adjacent to the tripyrimidine bulge in HIV-1 TAR results in a more pronounced kinking of the helix axis than a randomly chosen sequence (*53*). In a model of unbound ΔTAR generated from experimental data, the stacking of U23 introduces a kink in the helix axis, which changes direction by about 45° (*25*). This corresponds with the measured angle between the TAR helical stems of 50 ± 5° using transient electric birefringence (*54*).

In the bound form of ΔTAR, the two helical stems coaxially stack to form one continuous helix, accompanied by the unstacking and extrusion of the intervening bulge nucleotides. Coaxial stacking of helical stems has been reported in both HIV and BIV TAR RNAs upon binding of argininamide (*19*, *18*, *15*) and/or cognate peptides (*19*, *23*, *24*). A distortion in the position of the A22 base at the stacking junction reported here, where the A22 base is rolled into the major groove and tilted toward the G21-C41 base pair, has also been noted in another investigation (*19*). It is likely that the three extruded bulge nucleotides preclude a normal stacking arrangement of base pairs at the junction. In large part, the proton chemical shift changes reported here are consistent with those reported in other investigations (*19*, *15*). In most cases where differences exist, they are those of magnitude and not direction. In comparing observed chemical shift changes between the Tfr24−ΔTAR and TAR−argininamide complexes (*15*), the larger magnitudes of changes documented for the peptide−RNA complex may be due to specific contacts or generalized electrostatic effects of the peptide.

In contrast to the major unbound form of ΔTAR, the minor form exhibits a stable U40 imino proton and a strong NOE between the U40 imino and the A22 H2 protons. The nearly identical U40 imino proton chemical shifts of the bound and minor unbound forms of ΔTAR suggest a model for the conformation of the latter in which the two helices of ΔTAR stack coaxially and the three bulge nucleotides are extruded from the helix. This is also consistent with the A22 N1 and N3 chemical shifts of the minor form, which are similar to the other helical A nucleotides of ΔTAR [Figure 2(a)]. In a 1.3 Å crystal structure of unbound TAR RNA, a continuous helix is formed by coaxially stacked upper and lower helical stems (*55*). The bulge nucleotides adopt a novel extrahelical conformation that is stabilized by three divalent calcium ions, one of which interacts directly with three phosphate groups in the bulge region (*55*).

A base triple is formed between a bulge U, which we assume to be U23, and the A27-U38 base pair upon binding of the wild-type peptide. A stable U23 imino proton is observed in the wild-type complex, as are NOEs to U23 involving the A27 amino proton. The observation of a stable A27 amino proton in the peptide-bound form of ΔTAR suggests that the local environment of this proton is unique. Under identical conditions, other A amino protons in the bound form and all those in the unbound form of ΔTAR are not observed.

The existence of a U23-A27-U38 base triple in the bound form of TAR RNA is a subject of debate in the literature. Formation of the U23-A27-U38 base triple was first suggested in an NMR study of the HIV-1 TAR−argininamide complex by Williamson and co-workers (*15*). Although direct NMR evidence for the base triple was not observed in the HIV-1 TAR−argininamide complex, it was proposed on the basis of models generated with intermolecular NOEs to argininamide and internucleotide NOEs between U23 and G26 (*15*). Additional evidence for base triple formation came from NMR studies with mutated TAR RNA sequences that either favored base triple formation, including an isomorphous $C23^+$-G27-C38 triple mutant, or disrupted base triple formation in a TAR−argininamide complex (*16*). In the HIV-2 TAR−argininamide complex, a singlet corresponding to the A27 amino protons was observed at 750 MHz in a 3D NOESY−HSQC experiment at 5 °C (*18*). In an HIV-2 TAR $C23^+$-G27-C38 mutant−argininamide complex, however, C23 amino and protonated imino protons were observed (*17*). Significantly, observed NOEs between C23 amino and both G27 imino and C38 amino protons provide direct evidence for base triple formation (*17*).

Another detailed NMR investigation of HIV-1 TAR bound to argininamide and a Tat peptide including residues from the core and basic regions (ADP-1) maintains that the base triple is not formed in either case (*19*). However, NOEs place U23 in the major groove near G26 and A27. The reported apparent dissociation constants for ADP-1 and for a shorter peptide, ADP-5, which is equivalent to Tfr24, are 100 nM and 1 μM, respectively (*7*). We estimate an absolute dissociation constant for our Tfr24−ΔTAR complex of about 10 pM from kinetic association and dissociation rate constants (*32*). The anomalous differences in the values for binding affinity between the two groups suggest that one source of the discrepancy may be related to the nature of peptide preparations utilized in the two investigations (*7*).

A Hoogsteen base pairing arrangement in the bound form of ΔTAR between U23 and A27 agrees with mutational data suggesting that the N3 imino and the O4 carbonyl functional groups are critical for Tat binding and function. Replacement

of U23 with C23 or analogues with modified functionalities in the 3 and 4 positions abolished function in transactivation assays (*56*). Function was retained, however, with deoxyU at position 23 and in analogues where other ring positions were altered (*56*). Mutagenesis experiments have been used to examine the relative contributions of Watson−Crick and Hoogsteen pairing partners of the proposed base triple to specific arginine binding (*57*). The Hoogsteen interaction was shown to be critical for arginine binding whereas the Watson−Crick pairing was dispensable (*57*). In the model of the bound form of ΔTAR put forth by Varani and co-workers, U23 flanks one side of the specific argininamide binding pocket in the major groove (*19*). Despite the large amount of NMR data used in the structure determination, their model does not explain the critical nature of a U at position 23.

Tfr24-derived peptides with one or two arginines do not form the same complexes with TAR as the wild-type peptide as demonstrated via imino proton spectroscopy. The markers for specific complex formation observed for the wild-type complex are largely absent in these complexes. In light of the observation of multiple conformations for the bulge U nucleotides, it is likely that these peptides may form several complexes with TAR RNA by recognizing different bulged structures. This is corroborated by the result that the R52 peptide only discriminates wild-type TAR from TAR with a single bulged A residue and a bulgeless mutant by 2.5- and 4.3-fold, respectively (*32*).

Two related criteria must be fulfilled in order to obtain specific complex formation in the Tat peptide−TAR RNA system: stability of the complex toward dissociation and occupancy of TAR RNA arginine binding sites. The wild-type peptide meets both of these criteria. A single complex is produced between Tfr24 and TAR RNA, and this complex exhibits monophasic dissociation behavior (*32*). In the case of Tfr24 peptides with one or two arginines, it is likely that not all of the binding sites for guanidinium groups are saturated. In fact, the rapid and biphasic dissociation curves produced by these complexes suggest the formation of multiple complex species (*32*). Neither of the conditions for specific complex formation are satisfied by these model peptides. The case of argininamide is unique in that the criterion of arginine binding site saturation can be met by binding of multiple argininamides. Indeed, a 3 mM solution of argininamide is sufficient to elicit a specific conformational change in TAR RNA (*15*). However, the argininamide system lacks kinetic stability and is thus not suited for observation of the same alterations in base pairing and base stacking as observed for the wild-type complex.

The recognition of cognate RNA molecules by arginine-rich motif (ARM) proteins is a paradigm of the importance of RNA structure in RNA−protein interactions. The ARM proteins use a variety of structural motifs to recognize and bind their specific RNA targets. Although the small number of complexes examined in detail precludes the formation of a simple recognition code for the ARM proteins, the basis for such a code may be related to structural features of their cognate RNA binding sites. Frankel and co-workers have proposed that the structures adopted by ARM domains for RNA recognition are based on the width of the cognate RNA major groove (*58*). In their model, α-helices are used to recognize very wide major grooves at internal loop structures, whereas nonhelical or extended structures recognize narrower major grooves, where α-helical structures are sterically excluded (*58*). The bound structure of Tfr24 is presumably not α-helical. The CD difference spectrum of Tfr24 bound to ΔTAR does not contain the signature features of an α-helix (*32*). In addition, proline substitution mutations in the basic domain of HIV-1 Tat that abolish the potential for α-helix formation do not affect RNA-binding affinity in vitro or in vivo (*58*).

Adaptive binding is a theme common to the class of ARM protein−RNA interactions, where both partners in the interaction undergo conformational changes or stabilization upon complex formation. The peptides used as models of the entire proteins adopt a random coil conformation in the unbound state as evidenced by CD spectroscopy (*32*). NMR studies of HIV-1 Tat indicate that the basic domain also has a flexible conformation in the context of the entire protein (*59*). Investigations of the HIV-1 Rev−RRE and the HIV-1 TAR−arginine complexes have demonstrated that the specificity of the interactions can be modulated from both the protein and RNA sides, respectively (*60, 61*). Since the basic domain of the HIV-1 Rev protein can functionally substitute for the basic domain of Tat in a mutant Tat protein (*62*, *63*), the question arises as to whether the bound conformation of the Rev basic domain in this case is the same or different than that when bound to the cognate RRE RNA. If the RNA-bound structures of the ARM basic domains are determined by cognate RNA structure, an intriguing hypothesis is that some of these domains may be capable of folding into different conformations in response to different RNA structures.

The interaction between Tat and TAR is of considerable therapeutic interest. A potential design strategy for a class of inhibitor drugs to a particular ARM protein−RNA interaction would take adaptive binding into account, in that targeted sites would be those that would prevent the basic RNA recognition domain from folding into (or the cognate RNA from adopting) a functional bound conformation. Recent investigations of the λ N-box B and Ffh-4.5S RNA interactions suggest that RNA molecules may, in addition to serving as protein scaffolds, also affect protein function (*64*). Since a large number of RNA-binding proteins, including ribosomal proteins, contain a conserved arginine-rich motif, it is tempting to speculate that the flexibility embodied within these domains may be important for RNA-mediated regulation of both ribonucleoprotein assembly and biological function.

ACKNOWLEDGMENT

We thank Grace Sun for synthesis of deoxyribonucleotides. We acknowledge members of the W. M. Keck Foundation at Yale University School of Medicine, including Jim Elliot and Janet Crawford for peptide synthesis, and Myron Crawford and Kathy Stone for peptide amino acid analysis and mass spectrometry.

SUPPORTING INFORMATION AVAILABLE

Included are 8 NMR assignment tables, 7 NMR constraint files, and 1 RMSD value table for the unbound and Tat peptide-bound forms of ΔTAR RNA (27 pages). This

material is available free of charge via the Internet at http://pubs.acs.org.

REFERENCES

1. Cullen, B. R. (1986) *Cell 46*, 973−982.
2. Fisher, A. G., Feinberg, M. B., Josephs, S. F., Harper, M. E., Marselle, L. M., Reyes, G., Gonda, M. A., Aldovini, A., Debouk, C., Gallo, R. C., and Wong-Staal, F. (1986) *Nature 320*, 367−371.
3. Cullen, B. R., and Greene, W. C. (1989) *Cell 58*, 423−426.
4. Peterlin, B. M., Luciw, P. A., Barr, P. J., and Walker, M. D. (1986) *Proc. Natl. Acad. Sci. U.S.A. 83*, 9734−9738.
5. Muesing, M. A., Smith, D. H., and Capon, D. J. (1987) *Cell 48*, 691−701.
6. Weeks, K. M., Ampe, C., Schultz, S. C., Steitz, T. A., and Crothers, D. M. (1990) *Science 249*, 1281−1285.
7. Churcher, M. J., Lamont, C., Hamy, F., Dingwall, C., Green, S. M., Lowe, A. D., Butler, P. D. G., Gait, M. J., and Karn, J. (1993) *J. Mol. Biol. 230*, 90−110.
8. Weeks, K. M., and Crothers, D. M. (1991) *Cell 66*, 577−588.
9. Calnan, B. J., Tidor, B., Biancalana, S., Hudson, D., and Frankel, A. D. (1991b) *Science 252*, 1167−1171.
10. Pritchard, C. E., Grasby, J. A., Hamy, F., Zacharek, A. M., Singh, M., Karn, J., and Gait, M. J. (1994) *Nucleic Acids Res. 22*, 2592−2600.
11. Frankel, A. D. (1992) *Protein Sci. 1*, 1539−1542.
12. Calnan, B. J., Biancalana, S., Hudson, D., and Frankel, A. D. (1991a) *Genes Dev. 5*, 201−210.
13. Tao, J., and Frankel, A. D. (1992) *Proc. Natl. Acad. Sci. U.S.A. 89*, 2723−2726.
14. Tan, R., and Frankel, A. D. (1992) *Biochemistry 31*, 10288−10294.
15. Puglisi, J. D., Tan, R., Calnan, B. J., Frankel, A. D., and Williamson, J. R. (1992) *Science 257*, 76−80.
16. Puglisi, J. D., Chen, L., Frankel, A. D., and Williamson, J. R. (1993) *Proc. Natl. Acad. Sci. U.S.A. 90*, 3680−3684.
17. Brodsky, A. S., Erlacher, H. A., and Williamson, J. R. (1998) *Nucleic Acids Res. 26*, 1991−1995.
18. Brodsky, A. S., and Williamson, J. R. (1997) *J. Mol. Biol. 267*, 624−639.
19. Aboul-ela, F., Karn, J., and Varani, G. (1995) *J. Mol. Biol. 253*, 313−332.
20. Aboul-ela, F., Karn, J., and Varani, G. (1996) *Nucleic Acids Res. 24*, 3974−3981.
21. Holbrook, S. R., Sussman, J. L., Warrant, R. W., and Kim, S.-H. (1978) *J. Mol. Biol. 123*, 631−660.
22. Ye, X., Gorin, A., Ellington, A. D., and Patel, D. J. (1996) *Nat. Struct. Biol. 3*, 1026−1033.
23. Puglisi, J. D., Chen, L., Blanchard, S., and Frankel, A. D. (1995) *Science 270*, 1200−1203.
24. Ye, X., Kumar, R. A., and Patel, D. J. (1995) *Chem. Biol. 2*, 827−840.
25. Long, K. S. (1997) Ph.D. Thesis, Yale University, New Haven, CT.
26. Sundquist, W. I. (1996) *Nat. Struct. Biol. 3*, 8−11.
27. Milligan, J. F., Groebe, D. R., Witherell, G. W., and Uhlenbeck, O. C. (1987) *Nucleic Acids Res. 15*, 8783−8798.
28. Milligan, J. F., and Uhlenbeck, O. C. (1989) *Methods Enzymol. 180*, 51−62.
29. Nikonowicz, E. P., Sirr, A., Legault, P., Jucker, F. M., Baer, L. M., and Pardi, A. (1992) *Nucleic Acids Res. 20*, 4507−4513.
30. Batey, R. T., Inada, M., Kujawinski, E., Puglisi, J. D., and Williamson, J. R. (1992) *Nucleic Acids Res. 20*, 4515−4523.
31. Wain-Hobson, S., Sonigo, P., Danos, O., Cole, S., and Alizon, M. (1985) *Cell 40*, 9−17.
32. Long, K. S., and Crothers, D. M. (1995) *Biochemistry 34*, 8885−8895.
33. Kumar, A., Ernst, R. R., and Wüthrich, K. (1980) *Biochem. Biophys. Res. Commun. 95*, 1−6.
34. Piantini, U., Sørensen, O., and Ernst, R. R. (1982) *J. Am. Chem. Soc. 104*, 6800−6801.
35. Sklenár, V., and Bax, A. (1987) *J. Magn. Reson. 74*, 469−479.
36. Bax, A., Griffey, R. H., and Hawkins, B. L. (1983a) *J. Magn. Reson. 55*, 301−315.
37. Bax, A., Griggey, R. H., and Hawkins, B. L. (1983b) *J. Am. Chem. Soc. 105*, 7188−7190.
38. Grzesiek, S., and Bax, A. (1993) *J. Am. Chem. Soc. 115*, 12593−12594.
39. Lippens, G., Dhalluin, C., and Wieruszeski, J.-M. (1995) *J. Biomol. NMR 5*, 327−331.
40. Piotto, M., Saudek, V., and Sklenár, V. (1992) *J. Biomol. NMR 2*, 661−665.
41. Shaka, A. J., Barker, P. B., and Freeman, R. (1985) *J. Magn. Reson. 64*, 547−552.
42. Varani, G., Aboul-ela, F., and Allain, F. H.-T. (1996) *Prog. NMR Spectrosc. 29*, 51−127.
43. Saenger, W. (1984) *Principles of Nucleic Acid Structure*, Springer-Verlag, New York.
44. Sakore, T. D., Tavale, S. S., and Sobell, H. M. (1969) *J. Mol. Biol. 43*, 361−374.
45. Brünger, A. T. (1992) *X-PLOR, Version 3.1: A System for X-ray Crystallography and NMR*, Yale University Press, New Haven, CT.
46. Parkinson, G., Vojtechovsky, J., Clowney, L., Brünger, A. T., and Berman, H. M. (1996) *Acta Crystallogr. D52*, 57−64.
47. Wüthrich, K. (1986) *NMR of Proteins and Nucleic Acids*, John Wiley and Sons, Inc., New York.
48. Radhakrishnan, I., Gao, X., de los Santos, C., Live, D., and Patel, D. J. (1991) *Biochemistry 30*, 9022−9030.
49. Simorre, J.-P., Zimmermann, G. R., Pardi, A., Farmer, B. T., II, and Mueller, L. (1995) *J. Biomol. NMR 6*, 427−432.
50. King, G. C., Harper, J. W., and Xi, Z. (1995) *Methods Enzymol. 261*, 436−450.
51. Colvin, R. A., and Garcia-Blanco, M. A. (1992) *J. Virol. 66*, 930−935.
52. Bhattacharyya, A., Murchie, A. I. H., and Lilley, D. M. J. (1990) *Nature 343*, 484−487.
53. Riordan, F. A., Bhattacharyya, A., McAteer, S., and Lilley, D. M. J. (1992) *J. Mol. Biol. 226*, 305−310.
54. Zacharias, M., and Hagerman, P. J. (1995) *Proc. Natl. Acad. Sci. U.S.A. 92*, 6052−6056.
55. Ippolito, J. A., and Steitz, T. A. (1998) *Proc. Natl. Acad. Sci. U.S.A. 95*, 9819−9824.
56. Sumner-Smith, M., Roy, S., Barnett, R., Reid, L. S., Kuperman, R., Delling, U., and Sonenberg, N. (1991) *J. Virol. 65*, 5196−5202.
57. Tao, J., Chen, L., and Frankel, A. D. (1997) *Biochemistry 36*, 3491−3495.
58. Tan, R., and Frankel, A. D. (1995) *Proc. Natl. Acad. Sci. U.S.A. 92*, 5282−5286.
59. Bayer, P., Kraft, M., Ejchart, A., Westendorp, M., Frank, R., and Rösch, P. (1995) *J. Mol. Biol. 247*, 529−35.
60. Jain, C., and Belasco, J. G. (1996) *Cell 87*, 115−125.
61. Tao, J., and Frankel, A. D. (1996) *Biochemistry 35*, 2229−2238.
62. Southgate, C., Zapp, M. L., and Green, M. R. (1990) *Nature 345*, 640−642.
63. Subramanian, T., Kuppuswamy, M., Venkatesh, L., Srinivasan, A., and Chinnadurai, G. (1990) *Virology 176*, 176−183.
64. Frankel, A. D., and Smith, C. A. (1998) *Cell 92*, 149−151.

BI990590H